Tampere University of Applied Sciences

Please note! This is a self-archived version of the original article.

Huom! Tämä on rinnakkaistallenne.

To cite this Article / Käytä viittauksessa alkuperäistä lähdettä:

Mahlamäki, E., Schlapp-Hackl, I., Rissanen, M., Hummel, M. & Mäkelä, M. (2023) Discriminating the viscoelastic properties of cellulose textile fibers for recycling. Resources, Conservation and Recycling, 2023.

URL: https://doi.org/10.1016/j.resconrec.2023.106984

TAMPEREEN AMMATTIKORKEAKOULU
Kuntokatu 3, 33520 Tampere www.tuni.fi/tamk | p. 0294 5222

Resources, Conservation & Recycling 193 (2023) 106984

Contents lists available at ScienceDirect

Resources, Conservation & Recycling

journal homepage: www.elsevier.com/locate/resconrec

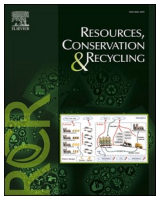

Full length article

Discriminating the viscoelastic properties of cellulose textile fibers for recycling

Ella Mahlamäki [a], Inge Schlapp-Hackl [b], Marja Rissanen [b], Michael Hummel [b], Mikko Mäkelä [a,*]

[a] VTT Technical Research Centre of Finland Ltd., PO Box 1000, 02044 VTT Espoo, Finland
[b] Aalto University, School of Chemical Engineering, Department of Bioproducts and Biosystems, PO Box 16300, 00076 Aalto, Finland

ARTICLE INFO

Keywords:
Cotton
Degree of polymerization
Discriminant analysis
Hyperspectral imaging
Intrinsic viscosity
Near infrared

ABSTRACT

The viscoelastic properties of cellulose fibers play an important role in chemical recycling of textiles. Here we discriminated the intrinsic viscosity of cotton roll towels and bed linens using near-infrared imaging spectroscopy and supervised pattern recognition. The classification results showed training and test set accuracies of 84–97% and indicated that the relevant spectral features were related to water, cellulose, and cellulose crystallinity. We hypothesized that the decreasing intrinsic viscosity of cotton was associated with changes in cellulose crystallinity and water adsorption, which was supported by additional X-ray and sorption measurements. These results are important as they indicate the potential to non-invasively estimate the degree of polymerization and the suitability of different cotton materials for chemical recycling. We propose that changes in the degree of polymerization and cellulose crystallinity could be used as an indicator of the chemical quality of cellulose fibers, which would have wider impacts for textile recycling.

1. Introduction

Chemical recycling of waste textiles into regenerated cellulose fibers is a promising step in meeting the increasing demand for textile fibers. The global fiber production for textiles has more than doubled to 120 million tons since the year 2000 (The Fiber Year, 2020). Over the same period the world population has grown by 25% (Palacios-Mateo et al., 2021) and the European Union and Switzerland alone currently generate 7–7.5 million tons of textile waste every year (McKinsey and Company, 2022). This equates to over 15 kg per capita and could increase to nearly 20 kg by 2030 (McKinsey and Company, 2022). Less than 15% of textile waste from clothing applications is currently recycled or reused, the majority is mainly landfilled or incinerated (The Ellen MacArthur Foundation, 2017). This disposed waste feedstock provides an opportunity to complement primary virgin fibers through recycling.

Fiber properties play an important role in chemical recycling of cellulose fibers. Cotton and regenerated cellulose, such as viscose and lyocell, show a polymorphic difference in their crystal structure and in polymer chain length (Makarem et al., 2019; Wedin et al., 2019). Polymer chain length, or the degree of polymerization, together with the molecular mass distribution govern the viscoelastic properties of dissolved fibers. These properties need to be controlled to manage spinning and regeneration behavior during recycling. Dissolved fiber properties can in practice be manipulated by changing the cellulose concentration in solution, by lowering the degree of polymerization of the fibers, or by blending the fibers with other feedstocks (Wedin et al., 2019). Merely estimating the viscoelastic behavior of fibers by measuring intrinsic viscosity with traditional laboratory methods is, however, time-consuming and expensive.

We have recently shown how virgin and regenerated cellulose fibers were identified using near infrared (NIR) imaging spectroscopy and chemometrics (Mäkelä et al., 2021). Our results together with the recent results of others (Rashed et al., 2021; Saito et al., 2021), were encouraging contributions to the textile identification field, which has mainly concentrated on synthetic and natural fibers (Blanch-Perez-del-Notario et al., 2019; Cura et al., 2021; Li et al., 2019; Mäkelä et al., 2020; Tan et al., 2019). Reliable identification of different cellulose fibers enables managing the logistics and feedstock supply for chemical recycling. Regenerated fibers show on average lower polymer chain lengths than virgin cotton, but mechanical and chemical degradation of textiles during service and laundering is known to decrease polymer chain length (Palme et al., 2014, 2016; Wedin et al., 2019). This uncontrolled, object-specific variation makes it difficult to control dissolved fiber rheology purely based on fiber type.

* Corresponding author.
E-mail address: mikko.makela@vtt.fi (M. Mäkelä).

https://doi.org/10.1016/j.resconrec.2023.106984
Received 4 October 2022; Received in revised form 9 March 2023; Accepted 27 March 2023
Available online 31 March 2023
0921-3449/© 2023 The Author(s). Published by Elsevier B.V. This is an open access article under the CC BY license (http://creativecommons.org/licenses/by/4.0/).

Here, we build on our previous work and illustrate how the intrinsic viscosity of cellulose fibers can be estimated by NIR imaging and supervised pattern recognition. Our method (Mahlamäki, 2022) takes advantage of averaging across individual pixel spectra to improve the stability of sample spectra for subsequent feature extraction and classification. We show how the classification enabled discriminating cotton fibers into specific viscosity ranges and discuss how further analysis of the classifier indicated changes in the relative crystallinity and water adsorption of cellulose with the degradation of the fibers. Overall, our results provide a means to non-invasively estimate the viscoelastic properties of cellulose fibers for chemical recycling and to potentially evaluate the chemical quality of textile fibers in the broader context of textile recycling.

2. Experimental

2.1. Samples and reference measurements

Two sets of cotton samples were acquired from known textile operators. The first set included 100% cotton bed linen fabrics used in hospitals and was provided by Uudenmaan Sairaalapesula Oy (Wang, 2018). The bed linens included 18 different fabrics and three to four samples were prepared per fabric, which generated a total of 55 samples. The second set was composed of 100% cotton roll towel fabrics and was provided by Lindström Oy. The roll towels included 19 different fabrics and three samples were prepared per fabric providing a total of 57 samples. All samples had physical dimensions of circa 10 × 10 cm^2.

The intrinsic viscosities of the samples were determined on the fabric level, which provided a total of 37 reference viscosities. Two to three additional 10 × 10 cm^2 pieces of the bed linens and roll towels were prepared from adjacent parts to the imaging samples and ground to 600-micron segments using a Wiley Mini Mill (Model 475-A) with a 30-mesh screen. The ground powders were combined, and two to three solutions were then prepared for determining intrinsic viscosity in triplicate according to the standard method SCAN—CM 15:99 (1988) of the Scandinavian pulp, paper, and board testing committee. Table 1 summarizes the materials, number of samples, and determined intrinsic viscosity ranges based on the means of the replicates. The determined intrinsic viscosities of the fabrics and their pooled standard deviations are given in Table S1 in the Supplementary information.

Cellulose crystallinity and water adsorption were determined from chosen bed linen fabrics. Small fragments of the samples were first milled, and their X-ray diffraction patterns were determined with a Xenocs Xeuss 3.0 X-ray diffractometer. The instrument was operated in transmission mode with Cu K_α radiation (λ = 1.54189 Å) at 50 kV/0.6 mA and was equipped with a Dectris Eiger2 R 1 M detector. The samples were placed into the radiation beam with a sample-to-detector distance of 56 mm under a vacuum of ca. 0.2 mbar. The powder diffraction data were collected from different spots of the sample in continuous mode from 5° to 50° 2θ using an exposure time of 480 s. The signals were corrected by subtracting background signals, which were recorded without any sample. The diffraction patterns were then analysed with the Fityk 1.3.1 (Softpedia®) software and the corresponding Segal crystallinity indices were determined according to Segal et al. (1959) and French (2014).

Water adsorption was determined using a dynamic vapor sorption analyzer (DVS Resolution, Surface Measurement Systems Ltd., UK). The fabrics were first dried at 50 °C for 5 h and stored in a desiccator. The mass change of approximately 15–20 mg of each sample was then determined by adjusting the relative humidity of the microbalance chamber stepwise from 20% to 80% at a temperature of 25 °C under a nitrogen flow of 200 ml min^{-1}. The relative humidity in the chamber was kept constant during each step until the sample mass reached equilibrium with a mass change lower than 0.002 mg min^{-1} over a 10-minute period. The water adsorption of three replicate samples were determined and the results were reported as the weight percent change of the dry fabrics.

Table 1
The materials, number of samples, and the determined intrinsic viscosity ranges.

Material	Fabrics	Overall samples	Measured intrinsic viscosities (ml g^{-1})
Cotton bed linens	18	55	300–1270
Cotton roll towels	19	57	590–1660

2.2. Imaging spectroscopy

NIR images of the textile samples were determined with a Specim SWIR 3 (Specim, Spectral Imaging, Ltd.) imaging spectrograph. The instrument operated in line-scanning mode and the detector recorded light intensity on 384 spatial pixels and 288 spectral variables. The wavelength range was 967–2560 nm with a sampling of 5.6 nm and a spectral resolution of 12 nm (full width half maximum). During the imaging procedure the samples moved under the camera and the speed of the moving stage was adjusted so that round objects appeared approximately round. The samples were illuminated with quartz halogen lamps and the field of view was set to approximately 12 cm. The integration time was adjusted so that the highest reflectance signals from an externally calibrated 99% reflectance target were approximately 90% of the maximum signal output. The images were first determined as raw signal intensity counts and were then converted to reflectance values using a two-point linear reflectance transformation based on reflectance target and dark current measurements (Burger and Geladi, 2005). Wavelength variables outside the range 1000–2500 nm were excluded to remove the noise at extreme wavelengths. This reduced the number of spectral variables to 270.

2.3. Data analyses

The samples in the reflectance images were separated from the backgrounds using principal component analysis (PCA) (Bro and Smilde, 2014; Geladi et al., 1989). All sample pixels were then used to calculate the average spectrum of each sample. The reflectance spectra were -$\log_{10}$ transformed into absorbance units and preprocessed using a second order and first derivative Savitzky-Golay polynomial filter with a window size of 15 variables followed by standard normal variate (SNV) transformation (Barnes et al., 1989; Burger and Geladi, 2007).

The differences in the sample spectra were first determined using PCA. The sample spectra were combined, mean centered, and decomposed according to the general PCA model, Eq. (1):

$$\mathbf{X} = \sum_{i=1}^{n} \mathbf{t_i} \mathbf{p_i}^{\mathbf{T}} + \mathbf{E_n} \quad (1)$$

where $\mathbf{X}$ denoted a matrix of preprocessed and mean centered average sample spectra, $\mathbf{t_i}$ and $\mathbf{p_i}$ the principal component score and loading vectors, respectively, and $\mathbf{E_n}$ the residual matrix after n principal components.

The samples were then classified into three different viscosity ranges using linear discriminant analysis (LDA) (Morais et al., 2020). The LDA procedure can be broken down into two separate steps. The training set scores on a chosen number of principal components were first projected into new canonical dimensions, which maximized separation between the defined classes. The scores on these dimensions were then used to determine the class centroids and the objects were assigned to the class with the closest centroid.

A pooled within-class covariance matrix was first determined to describe the variation within the classes, Eq. (2) (McLachlan, 1992):

$$\mathbf{W} = \frac{1}{n-c}\sum_{i=1}^{c}\sum_{j=1}^{n_i}(\mathbf{t_{ij}} - \bar{\mathbf{t}}_i)^{\mathrm{T}}(\mathbf{t_{ij}} - \bar{\mathbf{t}}_i) \quad (2)$$

where **W** denoted the within-class scatter matrix of the three groups, n the number of training objects, c the number of classes, n_i the number of training objects in the ith class, $\mathbf{t_{ij}}$ the PCA scores of the jth sample in ith class and $\bar{\mathbf{t}}_i$ the mean score vector of the ith class. A pooled between-class covariance matrix described the variation between the classes, Eq. (3) (McLachlan, 1992):

$$\mathbf{B} = \frac{1}{c-1}\sum_{i=1}^{c} n_i \bar{\mathbf{t}}_i^{\mathbf{T}}\bar{\mathbf{t}}_i \quad (3)$$

The new canonical dimensions were determined as the eigenvectors of $\mathbf{W}^{-1}\mathbf{B}$ by solving the eigenvalue problem, Eq. (4):

$$\mathbf{W}^{-1}\mathbf{B}\mathbf{L} = \mathbf{L}\lambda \quad (4)$$

where **L** denoted the eigenvectors and λ a diagonal matrix of the corresponding non-zero eigenvalues.

A classification rule was then defined as, Eq. (5):

$$\mathrm{d}_i(\mathbf{c}) = \min_{1<i<c} \mathrm{d}_i(\mathbf{c}) \quad (5)$$

with

$$\mathrm{d}_i(\mathbf{c}) = (\mathbf{c} - \bar{\mathbf{c}}_i)\mathbf{S}^{-1}(\mathbf{c} - \bar{\mathbf{c}}_i)^{\mathrm{T}} \quad (6)$$

where $\mathrm{d}_i(\mathbf{c})$ in Eqs. (5) and (6) expressed the squared Mahalanobis distance (De Maesschalck et al., 2000) between the vector object **c** and the class centroid $\bar{\mathbf{c}}_i$ in the canonical sub-space by assuming equal variance-covariance using a pooled estimate **S** similar to Eq. (2).

Previous work has shown that a cellulosic solute with an intrinsic viscosity of around 400–500 ml g^{-1} typically offers good spinnability in a Lyocell-type spinning process (Asaadi et al., 2016). As we had a limited number of samples in the exact 400–500 ml g^{-1} range, we defined the three viscosity ranges for classification as <350, 350–550, and >550 ml g^{-1}. Training and test sets were formed by allocating the samples from every third fabric object into a test set and the PCA model was determined based on the training set. The optimal number of principal components was determined by cross-validation. For cross-validation the fabric objects in the training group were consecutively divided into three groups and PCA-based classification models were built by leaving out the samples in each group once. The left-out group was used as a cross-validation test set and the share of correctly classified test objects was determined on each cross-validation round. The lowest number of principal components which produced the highest overall share of correctly classified test samples was then chosen. The analyses were performed using in-house scripts developed in Matlab® (The MathWorks, Inc.) including functions from the PLS toolbox (Eigenvector Research, Inc.).

3. Results and discussion

3.1. Technical details

The intrinsic viscosity of a cellulose substrate relates to the average degree of polymerization and is used to describe the viscoelastic properties of dissolved cellulose fibers. It is a key parameter that must be controlled to manage the spinning and regeneration behavior of textile fibers during chemical recycling. We preprocessed the average absorbance spectra of the cotton samples with Savitzky-Golay filtering and SNV transformation to emphasize the changes in the signals and to reduce the effects of inhomogeneous lighting and scattering. Fig. 1 shows the imaging principle and the effects of preprocessing on the sample spectra. As shown in Fig. 1C, the preprocessed and mean centered spectra contained information on chemical differences associated with the determined intrinsic viscosities. The moving window derivation in Savitzky-Golay filtering generated a peak shift and transformed the peaks in the original absorbance spectra into close to zero values in the preprocessed and mean centered spectra and the following PCA loadings.

The spectra were then decomposed into PCA scores and loadings for a systematic view on the differences within the samples. The first two

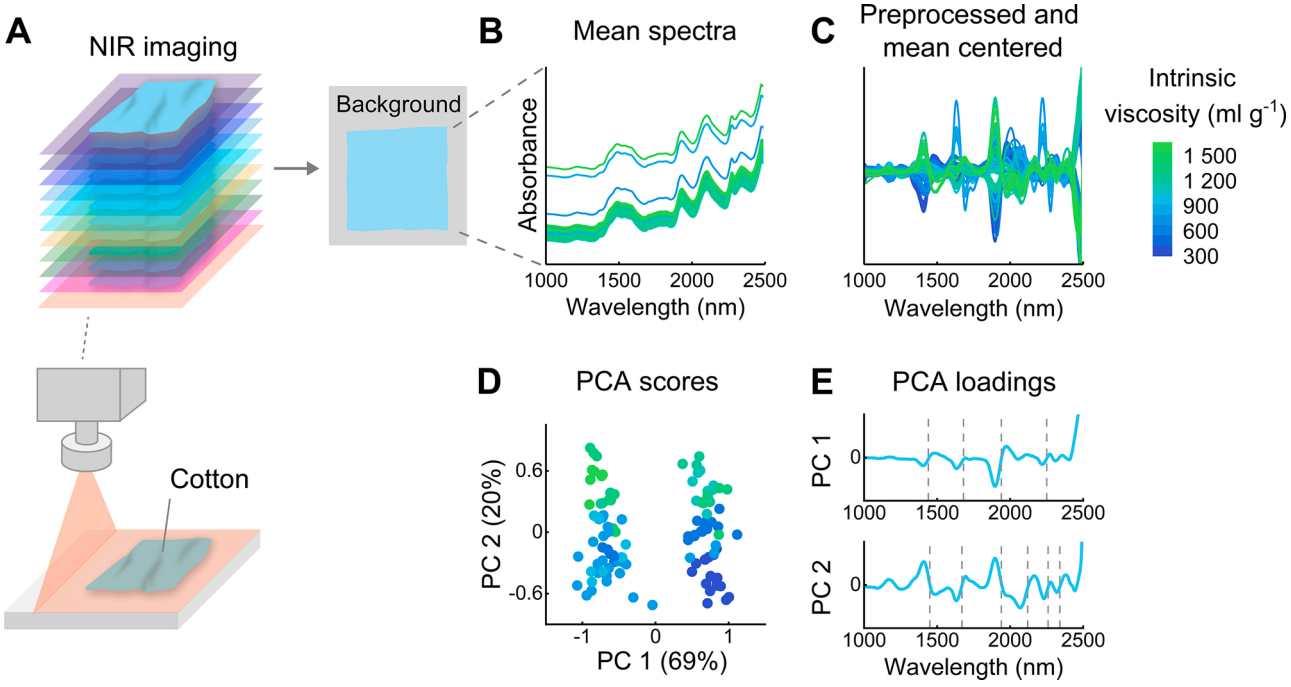

Fig. 1. An illustration of the imaging principle (A), average spectra of the samples (B), preprocessed and mean centered spectra (C), sample scores on the first two principal components (D), and respective principal component loadings with the most important wavelength differences (E). The wavelengths marked in (E) are discussed in the text and the spectra and symbols have been colored based on the measured intrinsic viscosities.

principal components explained 89% of the variation in the sample spectra. As illustrated in Fig. 1D, the score values indicated two distinct clusters based on fabric type. The cotton bed linens, which had on average lower intrinsic viscosities (Table 1), showed higher score values on the first principal component. The loadings indicated that these positive scores were associated with lower absorbance at approximately 1440 and 1940 nm (Fig. 1E), which generally correspond with the known water-related O—H vibrations in NIR spectra (Engelsen, 2016; Schwanninger et al., 2011). The loadings also showed absorbance differences at circa 1680 and 2250 nm, which suggested variation in the C—H, O—H and C—H vibrations previously reported for cellulose in wood (Schwanninger et al., 2011). Changes in intrinsic viscosity were also reflected in the PCA score values. As shown in Fig. 1D, scores on the second principal component increased towards higher intrinsic viscosity. The loadings suggested that the most important variations were located at approximately 1450, 1670, 1940, 2120, 2260, and 2340 nm in the original absorbance spectra (Fig. 1E). These wavelengths have been reported for the vibrational modes of O—H, C—H and C—O bonds in cellulose and other lignocellulosic components in wood (Schwanninger et al., 2011). Overall, the PCA results suggested that the spectral variation across both fabric types was associated with changes in the vibrational modes of water and cellulose.

The sample spectra were then divided into training and test sets for supervised classification. Important features in the training set were first extracted with PCA and the resulting scores were used for classification with LDA. The cross-validation results showed that 10 principal components provided the highest classification accuracy based on the training set, see Fig. S1 (Supplementary information). Too few principal components were unable to extract the underlying features which separated the classes, while too many generated dense training set clusters but decreased cross-validation accuracy. This indicated under- and over-fitting and emphasized the importance of extracting features for LDA with our dataset. We also determined cross-validation accuracy by using different preprocessing combinations based on first and second derivative Savitzky-Golay filtering and SNV (Xu et al., 2020). The results are shown in Fig. S2. The other preprocessing alternatives resulted in lower cross-validation accuracies and required more principal components for classification and were hence neglected.

The final LDA model resulted in overall classification accuracies of 97% and 84% based on the training and test sets, respectively. Fig. 2A illustrates the PCA scores projected onto the determined canonical dimensions and the class boundaries defined by equal Mahalanobis distances to the class centroids. Two training samples were misclassified to the viscosity class 350–550 ml g^{-1}. These two samples had reference intrinsic viscosities of 300 ± 20 and 600 ± 9 ml g^{-1} (mean ± standard deviation), which were relatively close to the defined limit values separating the three classes. The number of misclassified samples increased for the test set. Five test samples were misclassified to the viscosity class <350 ml g^{-1} and one test sample to the class 350–550 ml g^{-1}. These six misclassified samples originated from two distinct fabrics which had reference intrinsic viscosities of 380 ± 6 and 630 ± 18 ml g^{-1} (mean ± standard deviation). The former was close to the defined class limit (350 ml g^{-1}), while the latter showed a comparatively higher standard deviation in the determined reference values.

The overall accuracies were promising despite the class sizes, which were different across the classes. 78% of the overall samples were assigned to the viscosity class >550 ml g^{-1} and the remaining samples were distributed to the two other classes. We further divided the samples to training and test sets. The classifier was trained with only six samples in the 350–550 ml g^{-1} class and nine samples in the <350 ml g^{-1} class. We used overall accuracy determined as the share of correctly classified samples across the three classes to describe classification performance. Class-specific accuracies varied across the classes and were in the range 50–100% based on the test set, Fig. 2A. The lowest class-specific accuracy was determined from the 350–550 ml g^{-1} viscosity class and the highest from <350 ml g^{-1} class as shown by the test set results. Megahed et al. (2021) recently discussed the use of overall accuracy with imbalanced classes. Evaluating classifier performance with this metric can lead to an unjustified emphasis on the majority class during training, which can result in significantly higher test set accuracy with the majority class compared with the minority class (Megahed et al., 2021). These findings were not supported by our results, which showed lower class-specific accuracies with the majority and the other minority class. These misclassifications resulted from two distinct fabrics, where the determined reference values were likely not in line with the information contained in the spectra. Class imbalance could be compensated by collecting more samples to the low viscosity classes, which we aim to tackle in future work.

Canonical dimensions can be expressed as weights, which are useful to evaluate the importance of the extracted PCA features for class separation. We normalized these weights with the standard deviation of the principal component scores to account for the variation explained by each component. We then concentrated on the first canonical dimension and identified the components which were most influential for separating the viscosity classes (Fig. 2A). The results are shown in Fig. S3 and indicated that the first, second, seventh and ninth principal components were the most influential ones and played a key role in describing the class features in the spectra. The loadings of the first and second principal component were nearly identical to the ones shown in Fig. 1E as

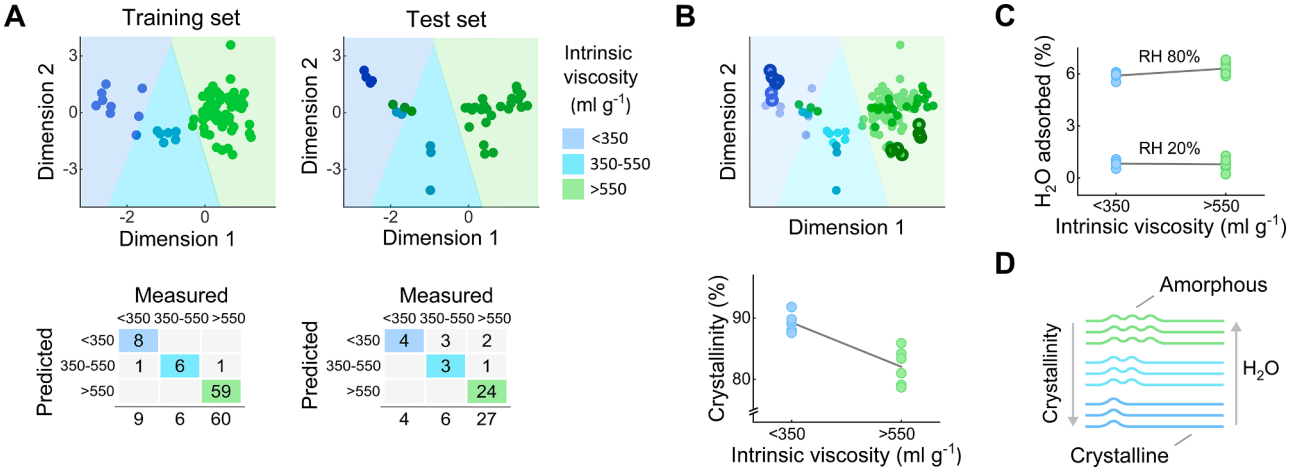

Fig. 2. Classification results for the training and test sets (A), samples chosen for the crystallinity measurements and their relative crystallinities (B), water adsorption by the chosen samples based on intrinsic viscosity and relative humidity (C), and a visualization of the proposed connection between intrinsic viscosity, cellulose crystallinity, and water adsorption in the cotton fabrics (D). The training and test sets scores in (A) have been super-imposed in (B) for clarity.

they were determined based on a similar but limited set of training spectra (Fig. S4). The seventh and ninth principal components provided additional information for evaluating the chemical changes between the classes. The majority of the original absorbance peaks indicated by the loadings were generated by the vibrational models of different chemical components in cellulose based on potential band assignments from the literature (Fig. S4). We identified additional wavelengths at circa 1490–1500 and 2080 nm, which coincided with the assignments for semi-crystalline or crystalline regions in wood cellulose (Belt et al., 2022; Mitsui et al., 2008; Schwanninger et al., 2011; Tsuchikawa et al., 2005). We note that the reliable assignment of NIR peaks is challenging as the specific literature on textile fibers is limited and imaging instruments have a lower spectral resolution than traditional spectrometers. The intensities of these peaks, however, seemed to increase in the original absorbance spectra with decreasing intrinsic viscosity and suggested a connection between intrinsic viscosity and cellulose crystallinity in the cotton fibers.

Changes in intrinsic viscosity were coupled to the vibrational modes of water, cellulose, and cellulose crystallinity based on the first canonical dimension and the PCA loadings. We hypothesized that a decrease in intrinsic viscosity, which is generally caused by the mechanical and chemical degradation of fibers, was associated with an increase in relative crystallinity due to the decomposition of amorphous or less-ordered cellulose (Palme et al., 2014, 2016). Fibers with higher intrinsic viscosity and lower relative crystallinity would be likely to adsorb more moisture as amorphous or less-ordered cellulose generally shows an increased number of adsorption sites due to improved structural accessibility (Ciolacu et al., 2012; Ioelovich, 2009). This hypothesis was supported by the higher water content in the roll towels with higher average viscosity based on the spectra. Increased moisture adsorption with decreasing cellulose crystallinity has previously been reported by studies on the moisture uptake of cellulose powders for pharmaceutical applications (Mihranyan et al., 2004; Heidarian Höckerfelt and Alderborn, 2014).

To test our hypothesis, we selected a total of twelve bed linen samples from four fabrics in the low and high viscosity classes within the viscosity range 310–1070 ml g^{-1} and determined their relative crystallinity and water adsorption using X-ray diffraction and dynamic vapor sorption. The results are given in Tables S2-S3. We then evaluated the effect of intrinsic viscosity on relative crystallinity and the effects of intrinsic viscosity and relative humidity on water adsorption using linear regression. Three observations, which showed distinctively different or physically meaningless values, were identified as outliers based on normalized model residuals and were excluded from the models (Figs. S5-S6, Tables S4-S5). As shown Fig. 2B, the low and high viscosity samples had average crystallinity indices of 89 ± 2% and 82 ± 3% (mean ± standard deviation) and the difference in these crystallinities was statistically significant ($p < 0.01$) based on the regression model (Fig. S7). Intrinsic viscosity and relative humidity also had a positive interaction effect on the water adsorption of the cotton bed linens based on vapor sorption. This interaction is illustrated in Fig. 2C and indicated that the bed linens with higher intrinsic viscosity and lower relative crystallinity adsorbed on average 0.4% more water under 80% relative humidity. The changes in adsorption were small across different intrinsic viscosities, but the interaction was statistically significant ($p = 0.08$) based on the regression model (Fig. S8). Overall, these crystallinity and sorption measurements were not successful in disproving our hypothesis. We have further visualized the proposed connection between intrinsic viscosity, cellulose crystallinity, and water adsorption in the cotton fabrics in Fig. 2D.

3.2. Environmental and economic relevance

These results are important as they indicate the potential to non-invasively estimate the degree of polymerization and the suitability of cotton materials for chemical recycling. We concentrated on two different fabric types to emphasize that the results were not limited to a specific material and could potentially be extended to other raw materials for chemical recycling. Our method could enable sorting these materials into different categories based on their macromolecular properties, which would allow tailoring the subsequent pretreatment conditions towards each category. Both chemical and enzymatic methods (Asaadi et al., 2016; Haslinger et al., 2019; Mölsä et al., 2022) are currently being developed for pretreating textile waste for chemical recycling. Tailoring the conditions of these methods would save both chemicals and energy and increase the competitiveness of chemical recycling. This would improve our ability to complement virgin textile fibers with chemically recycled waste fibers.

Mölsä et al. (2022) recently studied the environmental impacts of different management strategies for cotton roll towels. The authors compared a traditional linear life cycle with reuse and recycling alternatives by determining their climate change impact and water consumption. Their results showed that extending the lifetime of the roll towels has the largest potential to decrease the associated environmental impacts. Extending the number of the times the towels were used decreased the climate change impact and water consumption by 24% and 47%, respectively. The savings increased to 28% in climate change impact and 80% in water consumption if the towels were both reused and then chemically recycled, but the effects of recycling alone were more difficult to quantify. The savings potential of recycling was dependent on the chosen recycling technology and the type of substituted textile product. The highest savings were obtained by substituting conventional cotton.

Our results can have larger implications for different recycling pathways. In the future waste textiles will be mechanically, chemically, or thermally recycled depending on their composition and the requirements of the recycled products (Niinimäki et al., 2020). Virgin or regenerated cellulose fibers can be either mechanically or chemically recycled. As pointed out by Sahimaa et al. (2023), mechanical recycling requires shredding the fibers and decreases fiber quality but offers an alternative to replace part of the virgin fibers in a fabric. Chemical recycling demands additional water and chemicals but can even improve the strength properties of the fibers (Sahimaa et al., 2023). Both options will likely be used, and mechanically recycled fibers can be chemically regenerated after a certain number of lifecycles as the quality of the fibers decreases during mechanical recycling. We propose that changes in the degree of polymerization and cellulose crystallinity could be used as an indicator of the chemical quality of cellulose fibers to evaluate when the fibers require regeneration. According to our better knowledge such methods do not currently exist, and our approach described here could offer a viable alternative for further development.

4. Conclusions

We discriminated the viscoelastic properties of cotton bed linens and roll towels based on imaging spectroscopy and supervised pattern recognition. Changes in the intrinsic viscosity of cotton were visible in the average image spectra, which were classified into different viscosity ranges with discriminant analysis. The results showed overall classification accuracies of 84–97% based on the training and test sets and indicated that the relevant spectral features were related to water, cellulose, and cellulose crystallinity. We presented a hypothesis where a decrease in the intrinsic viscosity of cotton fibers was associated with changes in cellulose crystallinity and water adsorption. Additional X-ray and vapor sorption measurements showed that bed linens with higher intrinsic viscosity had on average lower relatively crystallinity and adsorbed more water under higher relative humidity therefore supporting our hypothesis. Our results are significant as they indicate the potential to non-invasively estimate the degree of polymerization and the suitability of cotton materials for chemical recycling across different material types. In the future this would allow tailoring the conditions of different pretreatments for chemical recycling of textile wastes. Finally,

we propose that changes in the degree of polymerization and cellulose crystallinity could be used as an indicator of the chemical quality of cellulose fibers, which would have wider impacts for different recycling methods within the circular economy of textiles.

CRediT authorship contribution statement

Ella Mahlamäki: Software, Validation, Formal analysis, Investigation, Data curation, Writing – original draft, Writing – review & editing, Visualization. **Inge Schlapp-Hackl:** Conceptualization, Methodology, Investigation, Resources, Writing – review & editing, Project administration. **Marja Rissanen:** Conceptualization, Methodology, Resources, Writing – review & editing. **Michael Hummel:** Supervision, Writing – review & editing. **Mikko Mäkelä:** Conceptualization, Methodology, Software, Validation, Resources, Writing – original draft, Writing – review & editing, Supervision, Project administration, Funding acquisition.

Declaration of Competing Interest

The authors declare the following financial interests/personal relationships which may be considered as potential competing interests: VTT Technical Research Centre of Finland Ltd. and Aalto University have a submitted a patent application (FI220225430) related to this work.

Data availability

The data that has been used is confidential.

Acknowledgements

Yingfeng Wang and Teemu Airaksinen from Aalto University, School of Chemical Engineering are gratefully acknowledged for measuring the intrinsic viscosity of the cotton bed linens and roll towels. This work was financially supported by the Strategic Research Council of the Academy of Finland under grant agreement no. 327296 – the FINIX project (finix.aalto.fi).

Supplementary materials

Supplementary material associated with this article can be found, in the online version, at doi:10.1016/j.resconrec.2023.106984.

References

Asaadi, S., Hummel, M., Hellsten, S., Härkäsalmi, T., Ma, Y., Michud, A., Sixta, H., 2016. Renewable high-performance fibers from the chemical recycling of cotton waste utilizing an ionic liquid. ChemSusChem 9, 3250–3258.
Barnes, R.J., Dhanoa, M.S., Lister, S.J., 1989. Standard normal variate transformation and de-trending of near-infrared diffuse reflectance spectra. Appl. Spectrosc. 43, 772–777.
Belt, T., Awais, M., Mäkelä, M., 2022. Chemical characterization and visualization of progressive brown rot decay of wood by near infrared imaging and multivariate analysis. Front. Plant Sci. 13, 940745.
Blanch-Perez-del-Notario, C., Saeys, W., Lambrechts, A., 2019. Hyperspectral imaging for textile sorting in the visible-near infrared range. J. Spectral Imaging 8, a17.
Bro, R., Smilde, A.K., 2014. Principal component analysis. Anal. Methods 6, 2812–2831.
Burger, J., Geladi, P., 2005. Hyperspectral NIR image regression part I: calibration and correction. J. Chemom. 19, 355–363.
Burger, J., Geladi, P., 2007. Spectral pre-treatments of hyperspectral near infrared images: analysis of diffuse reflectance scattering. J. Near Infrared Spectrosc. 15, 29–37.
Ciolacu, D., Pitol-Filho, L., Ciolacu, F., 2012. Studies concerning the accessibility of different allomorphic forms of cellulose. Cellulose 19, 55–68.
Cura, K., Rintala, N., Kamppuri, T., Saarimäki, E., Heikkilä, P., 2021. Textile recognition and sorting for recycling at an automated line using near infrared spectroscopy. Recycling 6, 11.
De Maesschalck, R., Jouan-Rimbaud, D., Massart, D.L., 2000. The Mahalanobis distance. Chemom. Intell. Lab. Syst. 50, 1–18.
Engelsen, S.B., 2016. Near infrared spectroscopy - a unique window of opportunities. NIR news 27, 14–17.
The Ellen MacArthur Foundation, 2017. A new textiles economy: redesigning fashion's future. Available at: https://ellenmacarthurfoundation.org/a-new-textiles-economy [accessed 23rd September 2022].
French, A.D., 2014. Idealized powder diffraction patterns for cellulose polymorphs. Cellulose 21, 885–896.
Geladi, P., Isaksson, H., Lindqvist, L., Wold, S., Esbensen, K., 1989. Principal component analysis multivariate images. Chemom. Intell. Lab. Syst. 5, 209–220.
Haslinger, S., Wang, Y., Rissanen, M., Lossa, M.B., Tanttu, M., Ilen, E., Määttänen, M., Harlin, A., Hummel, M., Sixta, H., 2019. Recycling of vat and reactive dyed textile waste to new colored man-made cellulose fibers. Green Chem 21, 5598.
Heidarian Höckerfelt, M., Alderborn, G., 2014. The crystallinity of cellulose controls the physical distribution of sorbed water and the capacity to present water for chemical degradation of a solid drug. Int. J. Pharm. 477, 326–333.
Ioelovich, M., 2009. Accessibility and crystallinity of cellulose. Bioresources 4, 1168–1177.
Li, J., Meng, X., Wang, W., Xin, B., 2019. A novel hyperspectral imaging and modeling method for the component identification of woven fabrics. Text. Res. J. 89, 3752–3767.
Mahlamäki, E., 2022. Hyperspectral Imaging to Estimate Intrinsic Viscosity of Cellulose-Based Fabrics. Faculty of Engineering and Natural Sciences. Tampere University, p. 61.
Makarem, M., Lee, C.H., Kafle, K., Huang, S., Chae, I., Yang, H., Kubicki, J.D., Kim, S.H., 2019. Probing cellulose structures with vibrational spectroscopy. Cellulose 26, 35–79.
The Fiber Year, 2020. The fiber year 2020 – world survey on textiles & nonwovens. Available for purchase at: https://thefiberyear.com/home/[accessed 23rd September 2022].
McKinsey & Company, 2022. Scaling textile recycling in Europe—Turning waste into value. Available at: https://www.mckinsey.com/industries/retail/our-insights/scaling-textile-recycling-in-europe-turning-waste-into-value [accessed 23rd September 2022].
McLachlan, G.J., 1992. Discriminant Analysis and Statistical Pattern Recognition. John Wiley & Sons, Inc., Hoboken, New Jersey.
Megahed, F.M., Chen, Y.-J., Megahed, A., Ong, Y., Altman, N., Krzywinski, M., 2021. The class imbalance problem. Nat. Methods 18, 1269–1272.
Mihranya, A., Llagostera, A.P., Karmhag, R., Strømme, M., Ek, R., 2004. Moisture sorption by cellulose powders of varying crystallinity. Int. J. Pharm. 269, 433–442.
Mitsui, K., Inagaki, T., Tsuchikawa, S., 2008. Monitoring of hydroxyl groups in wood during heat treatment using NIR spectroscopy. Biomacromolecules 9, 286–288.
Mäkelä, M., Rissanen, M., Sixta, H., 2020. Machine vision estimates the polyester content of recyclable waste textiles. Resour. Conserv. Recycl. 161, 105007.
Mäkelä, M., Rissanen, M., Sixta, H., 2021. Identification of cellulose textile fibers. Analyst 146, 7503–7509.
Mölsä, K., Horn, S., Dahlbo, H., Rissanen, M., 2022. Linear, reuse or recycling? An environmental comparison of different life cycle options for cotton roller towels. J. Clean. Prod. 374, 133976.
Morais, C.L.M., Lima, K.M.G., Singh, M., Martin, F.L., 2020. Tutorial: multivariate classification for vibrational spectroscopy in biological samples. Nat. Protoc. 15, 2143–2162.
Niinimäki, K., Peters, G., Dahlbo, H., Perry, P., Rissanen, T., Gwilt, A., 2020. The environmental price of fast fashion. Nat. Rev. Earth Environ. 1, 189–200.
Palacios-Mateo, C., van der Meer, Y., Seide, G., 2021. Analysis of the polyester clothing value chain to identify key intervention points for sustainability. Environ. Sci. Eur. 33, 2.
Palme, A., Idström, A., Nordstierna, L., Brelid, H., 2014. Chemical and ultrastructural changes in cotton cellulose induced by laundering and textile use. Cellulose 21, 4681–4691.
Palme, A., Theliander, H., Brelid, H., 2016. Acid hydrolysis of cellulose fibers: comparison of bleached kraft pulp, dissolving pulps and cotton textile cellulose. Carbohydr. Polym. 136, 1281–1287.
Rashed, H.S., Mishra, P., Nordon, A., Palmer, D.S., Baker, M.J., 2021. A comparative investigation of two handheld near-ir spectrometers for direct forensic examination of fibres in-situ. Vib. Spectrosc. 113, 103205.
Sahimaa, O., Miller, E.M., Halme, M., Niinimäki, K., Tanner, H., Mäkelä, M., Rissanen, M., Härri, A., Hummel, M., 2023. The only way to fix fast fashion is to end it. Nat. Rev. Earth Environ. 4, 137–138.
Saito, K., Yamagata, T., Kanno, M., Yoshimura, N., Takayanagi, M., 2021. Discrimination of cellulose fabrics using infrared spectroscopy and newly developed discriminant analysis. Spectrochim. Acta, Part A 257, 119772.
Schwanninger, M., Rodrigues, J.C., Fackler, K., 2011. A review of band assignments in near infrared spectra of wood and wood components. J. Near Infrared Spectrosc. 19, 287–308.
Segal, L., Creely, J.J., Martin Jr., A.E., Conrad, C.M., 1959. An empirical method for estimating the degree of crystallinity of native cellulose using the X-ray diffractometer. Text. Res. J. 29, 786–794.
Tan, C., Chen, H., Lin, Z., Wu, T., 2019. Category identification of textile fibers based on near-infrared spectroscopy combined with data description algorithms. Vib. Spectrosc. 100, 71–78.
Tsuchikawa, S., Yonenobu, H., Siesler, H.W., 2005. Near-infrared spectroscopic observation of the ageing process in archaeological wood using a deuterium exchange method. Analyst 130, 379–384.

Wang, Y., 2018. Simultaneous Recycling of Cellulose Fibers and Dyes from Dyed Cotton Waste in the Form of Dyed Lyocell fibers, Master's Programme in Chemical. Biochemical and Materials Engineering. Aalto University, p. 56.

Wedin, H., Lopes, M., Sixta, H., Hummel, M., 2019. Evaluation of post-consumer cellulosic textile waste for chemical recycling based on cellulose degree of polymerization and molar mass distribution. Text. Res. J. 89, 5067–5075.

Xu, J.-.L., Riccioli, C., Herrero-Langreo, A., Gowen, A.A., 2020. Deep learning classifiers for near infrared spectral imaging: a tutorial. J. Spectr. Imaging 9, a19.